Applied Catalysis B: Environmental 238 (2018) 236–247

Contents lists available at ScienceDirect

Applied Catalysis B: Environmental

journal homepage: www.elsevier.com/locate/apcatb

Synthesis and catalytic performance of $Cu_1Mn_{0.5}Ti_{0.5}O_x$ mixed oxide as low-temperature NH_3-SCR catalyst with enhanced SO_2 resistance

Qinghua Yan[a,b], Sining Chen[a], Cheng Zhang[a], Qiang Wang[a,*], Benoit Louis[b,*]

[a] College of Environmental Science and Engineering, Beijing Forestry University, 35 Qinghua East Road, Haidian District, Beijing 100083, PR China
[b] Laboratoire de Synthèse, Réactivité Organiques et Catalyse, Institut de Chimie, UMR 7177, Université de Strasbourg, 1 rue Blaise Pascal, 67000 Strasbourg, France

ARTICLE INFO

Keywords:
Selective catalytic reduction
Mn-based catalyst
Layered double hydroxides
SO_2 resistance
Regenerability

ABSTRACT

A new type of low-temperature NH_3-SCR catalyst with a chemical composition of $Cu_wMn_yTi_{1-y}O_x$ was prepared from layered double hydroxides precursors for the first time. The purpose of this novel design is to improve the De-NO_x efficiency and SO_2 resistance of Mn-based catalysts. The $Cu_1Mn_{0.5}Ti_{0.5}O_x$ catalyst achieved a NO_x conversion as high as 90% at 200 °C, which is much higher than that of the control catalysts Cu-Mn/TiO_2 (86.1%) and Mn/TiO_2 (80.7%). The properties of catalysts were characterized in detail using a series of physico-chemical techniques including XRD, BET, FTIR, SEM, TEM, H_2-TPR, NH_3-TPD, TGA, and XPS analyses. The excellent catalytic performance of $Cu_1Mn_{0.5}Ti_{0.5}O_x$ catalyst can be associated with its higher specific surface area and surface acidity, and more active MnO_2 and CuO species. Besides, when copper oxide is introduced, the catalysts showed significant resistance to 100 ppm SO_2 and 5% H_2O. Finally, the poisoning mechanism and the regenerability of $Cu_1Mn_{0.5}Ti_{0.5}O_x$ catalyst was proposed. In short, the newly designed $Cu_1Mn_{0.5}Ti_{0.5}O_x$ catalyst was found to have higher catalytic activity and excellent SO_2 and H_2O resistance compared to the control catalysts of Cu-Mn/TiO_2 and Mn/TiO_2.

1. Introduction

In order to fulfill the new and stricter regulations, many pollutant control technologies have been widely used to reduce the emission of air pollutants. The selective catalytic reduction (SCR) of NO_x with NH_3 (NH_3-SCR) is an efficient technique for removing NO_x from flue gases of power plant [1]. Commercial SCR catalysts (e.g. V_2O_5-WO_3/TiO_2) are always placed prior to dust precipitation and desulphurization system, and the high concentration of SO_2 and dust normally reduce the performance and durability of catalysts [2]. Therefore, a tail-end configuration is becoming attractive and the development of a suitable catalyst for low temperature (i.e. 140–200 °C) environment is crucial [3].

Over the past decade, great interest has been drawn on the research of low temperature SCR catalysts containing transition metal oxide catalysts such as CuO/TiO_2, Fe_2O_3/TiO_2, and MnO_x/TiO_2 [4–9]. Among them, Mn-based catalysts have shown excellent De-NO_x property under low-temperature sulfur-free conditions [10,11]. Under the actual SCR conditions, the stability of sulfates formed on TiO_2 surface is weaker than that on other supports such as ZrO_2 and Al_2O_3. Therefore, TiO_2 is believed to be a more SO_2-resistant support than other mixed oxides [12–14]. However, Mn/TiO_2 catalyst still has some problems, for example, easy sintering, poor thermal stability, and short lifetime, etc. Especially, during the preparation of Mn/TiO_2 catalyst, sintering easily occurs, resulting in a poor dispersion of active component. Many studies have shown that the Cu-Ti mixed oxide was a potential catalyst for HC-SCR with excess oxygen [15–19]. In addition, the Cu-based catalysts are more SO_2-resistant. Since the conventional impregnation preparation method often results in aggregated Mn oxides and relatively low catalytic activity, thus new synthesis methods for obtaining highly dispersed active components are highly desired.

Layered double hydroxides (LDHs) are a class of ionic lamellar compounds made up of positively charged brucite-like layers, with an interlayer region containing charge compensating anions and solvation molecules. LDHs have been suggested as a promising precursor for the preparation of highly dispersed mixed oxides with many good properties [20–24]. The layered double oxides (LDOs) obtained by calcination of LDHs normally consist highly dispersed active components, which possess better sintering-resistant property [25]. Thus, we propose that by optimizing the chemical composition of catalyst and using LDHs as precursor, a new catalyst $Cu_wMn_yTi_{1-y}O_x$ containing MnO_x and CuO as active components and TiO_2 as support can be designed. And such newly designed SCR catalyst should possess higher catalytic activity and better SO_2-resistant and sintering-resistant properties.

In this work, $Cu_wMn_yTi_{1-y}O_x$ catalysts with different contents of Cu,

* Corresponding authors.
E-mail addresses: qiangwang@bjfu.edu.cn (Q. Wang), blouis@unistra.fr (B. Louis).

https://doi.org/10.1016/j.apcatb.2018.07.035
Received 24 March 2018; Received in revised form 25 June 2018; Accepted 9 July 2018
Available online 11 July 2018

Mn, and Ti were prepared from the corresponding LDH precursors. All samples were carefully characterized using a series of techniques including X-ray powder diffraction (XRD), Fourier transform infrared spectroscopy (FTIR), scanning electron microscope (SEM), transmission electron microscopy (TEM), and BET analysis. The NH_3-SCR catalytic activity of catalysts were evaluated in the range of 100–250 °C. The influence of SO_2 and H_2O on the performance of catalysts were also investigated and compared with the conventional Mn/TiO_2 and Cu-Mn/TiO_2 catalysts. Finally, the involved mechanism was studied using X-ray photoelectron spectroscopy (XPS), in situ-diffuse reflectance infrared Fourier transform spectroscopy (in situ-DRIFTS), thermogravimetric analysis (TGA), NH_3-temparature programmed desorption (NH_3-TPD), SO_2-temparature programmed desorption (SO_2-TPD), and H_2-temperature programmed reduction (H_2-TPR).

2. Experimental

2.1. Preparation of $Cu_wMn_yTi_{1-y}O_x$, Cu-Mn/TiO_2, and Mn/TiO_2

The standard co-precipitation method is used to synthesize the $Cu_wMn_yTi_{1-y}$-CO_3 LDHs precursors. Hydroxyl ions (OH^-) and carbonates (CO_3^{2-}) were continuously supplied by the decomposition of urea in water. $Cu(NO_3)_2{\cdot}6H_2O$ (Sinopharm Chemical Reagent Co., Ltd.), 50% $Mn(NO_3)_2$ (Sinopharm Chemical Reagent Co., Ltd.) and titanium propoxide (Alfa Aesar) were used as metal precursors with various ratios of w and y (w = 0.5–3, y = 0.25–0.75). The mixed solution was stirred at 90 °C for 2 days. The synthetic precipitate was thoroughly washed with deionized water and then dried at 60 °C for 12 h. $Cu_wMn_yTi_{1-y}$-CO_3 LDHs were calcined at 400 °C for 5 h to obtain $Cu_wMn_yTi_{1-y}O_x$ catalyst. A more detailed preparation process of LDHs has been reported in many literature [26,27]. 20 wt% Mn/TiO_2, 10 wt% Cu-10 wt% Mn/TiO_2 20 wt% Cu-20 wt% Mn/TiO_2, and 40 wt% Cu-20 wt% Mn/TiO_2 were also prepared using the traditional incipient wetness method as control catalysts.

2.2. Catalyst characterization

Powder XRD was used to analyze the synthesized and calcined samples using a reflection mode of Cu Ka radiation on a Shimadzu XRD-7000 instrument. The chemisorption analyzer (SSA-7000, Builder) was used to measure the BET specific surface area (SSA) of samples. The morphologies of samples were characterized using field emission scanning electron microscope (FE-SEM, SU-8010, Hitachi). High resolution transmission electron microscopy (HR-TEM) analyses were performed on Tecnai G2 F20 (FEI, USA), with an accelerating voltage of 200 kV. Thermo Scientific Escalab 250Xi instrument was used for XPS analysis using monochromatic Al kα radiation ($h\nu$ = 1486.6 eV) at 15 kW accelerating power. The chemisorption analyzer (PCA-1200, Builder) was used for NH_3-TPD, SO_2-TPD, $SO_2 + NH_3 + O_2$-TPD, and H_2-TPR analyses.

Q50 TGA (TA Instruments) was used to perform thermogravimetric analysis of samples. In a flowing nitrogen (60 mL/min), the furnace temperature was raised to 800 °C at a rate of 10 °C/min. The FTS 3000 MX FTIR spectrophotometer (Bruker Vertex 70) was used to perform FTIR analysis using diamond ATR technology. The in situ DRIFT characterization was also implemented on the FTS 3000 MX FTIR (Bruker Vertex 70) spectrophotometer with a reaction cell (ZnSe windows) and a diffuse reflectance attachment (HARRICK). The resolution was 4 cm^{-1}, the number of scans was 32, the spectra were expressed as Kubelka–Munk function, and the background spectrum of catalyst was recorded in N_2.

2.3. Catalytic activity measurements

The NH_3-SCR catalytic experiments of synthesized catalysts were carried out in a fixed-bed stainless steel reactor at a flow rate of 200 mL/min loaded with 150 mg catalyst. The inlet gas contained 500 ppm NH_3, 500 ppm NO_x (about 480 ppm NO, and 20 ppm NO_2), 100 ppm SO_2 (if needed), 5% H_2O (if needed), and 5% O_2 with Ar as balance. The NO_x analyzer (Thermo Scientific 42i-HL, USA) was used to monitor the NO_x concentrations on-line, and the quadrupole mass spectrometer (QGA, Hidden, UK) was used to assess the N_2 selectivity. The NO_x conversion and N_2 selectivity at the steady state were obtained using the follow Eqs. (1) and (2).

$$NO_x\text{conversion} = \left(1 - \frac{NO_x(out)}{NO_x(in)}\right) \times 100\% \quad (1)$$

$$N_2\text{selectivity} = \left(1\text{-}\frac{2N_2O(out)}{NO_x(in) + NH_3(in) - NO_x(out) - NH_3(out)}\right) \times 100\% \quad (2)$$

3. Results and discussion

3.1. Characterization of samples

First, in order to confirm the successful synthesis of $Cu_wMn_yTi_{1-y}$-CO_3 LDHs, powder XRD analyses were performed. Fig. 1 shows the XRD patterns of $Cu_wMn_yTi_{1-y}$-CO_3 LDHs with the same Mn/Ti of 1 but different Cu/(Mn + Ti) molar ratios of 0.5, 1, 2, and 3. Four precursors all exhibited the characteristic diffraction peaks of LDHs structure without any impurity phase. The diffraction peaks at 2θ = 12.8°, 25.8°, 36.5°, 39.1°, 43.6°, 53.1°, and 63.1° can be attributed to the reflections of (003), (006), (012), (009), (015), (018), and (110) planes for $Cu_wMn_yTi_{1-y}$-CO_3 LDHs phase, respectively.

The specific surface area (SSA) is an important parameter for the performance of catalysts, thus the BET analyses of LDHs, LDOs, Cu-Mn/TiO_2, and Mn/TiO_2 were performed and summarized in Table 1. The SSA of $Cu_wMn_yTi_{1-y}$-CO_3 LDHs became higher from 86.6 to 113.5 m^2/g with the increase in molar ratio of Cu/(Mn + Ti). After calcination, the SSA of obtained mixed oxides were slightly decreased to the range of 56–102.1 m^2/g. It should be noted that Cu-Mn/TiO_2 catalyst possesses a larger specific surface area than Mn/TiO_2, indicating that the introduction of copper increased the specific surface area of catalysts [10,28]. Among all mixed oxides, $Cu_1Mn_{0.5}Ti_{0.5}O_x$ showed the highest SSA. It is well known that higher SSA could provide more available active sites on the catalyst surface for the reactants to participate in the reactions.

In addition, to better illustrate the structure of synthesized $Cu_wMn_yTi_{1-y}$-CO_3 LDHs, FTIR analyses were further conducted, as shown in Fig. 1(c). All samples exhibited similar FTIR spectra to Mg-Al hydrotalcite. The stretching vibrations of −OH groups at 3350 cm^{-1}, the angular deformation vibration of H_2O molecules at 1420 cm^{-1}, and the vibrations of carbonate ions at 1311 cm^{-1} were observed. The bands at about 866 and 497 cm^{-1} can be attributed to M−O (M−OH, O−M−O or M−O−M) vibrations [21,29–32]. Thus, both XRD and FTIR data confirmed the successful synthesis of $Cu_wMn_yTi_{1-y}$-CO_3 LDHs. In addition, after calcination, $Cu_wMn_{0.5}Ti_{0.5}O_x$ is mainly present in the CuO phase (Fig. 1(d)), and the related Mn phase almost did not be observed. This is probably because Mn oxide exists in a highly dispersed state.

The morphology of LDHs was revealed by SEM analyses. Fig. 2(a) shows that $Cu_{0.5}Mn_{0.5}Ti_{0.5}$-CO_3 LDH possesses nanoplatelets morphology assembled together, a typical morphology for LDHs. Fig. 2(b) shows the HR-TEM image of the $Cu_1Mn_{0.5}Ti_{0.5}O_x$ catalyst. A lattice fringe with a spacing distance of 0.25 nm was observed, which can be referenced to the (−111) crystal plane of CuO. These data further suggested that $Cu_wMn_yTi_{1-y}$-CO_3 LDH was successfully synthesized, and thermal treatment can lead to the formation of highly dispersed CuO species, which agrees well with the results of XRD.

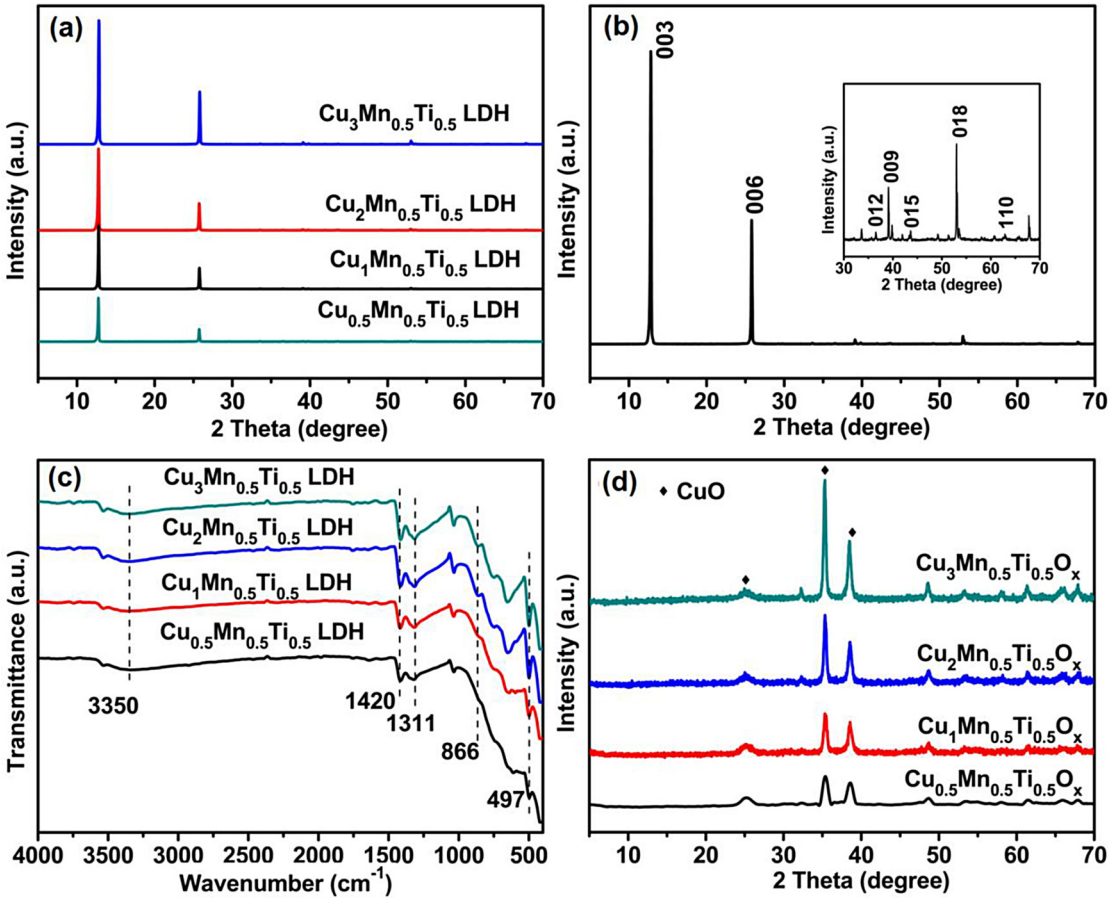

Fig. 1. (a) XRD patterns of $Cu_wMn_yTi_{1-y}$-CO_3 LDHs with different Cu/(Mn + Ti) ratios from 0.5 to 3, (b) XRD pattern of $Cu_wMn_{0.5}Ti_{0.5}$-CO_3 LDH with Cu/(Mn + Ti) = 1, (c) FTIR spectra of $Cu_wMn_yTi_{1-y}$-CO_3 LDHs with different Cu/(Mn + Ti) ratios, and (d) XRD patterns of $Cu_wMn_{0.5}Ti_{0.5}O_x$ LDOs with different Cu/(Mn + Ti) ratios obtained by calcining at 400 °C.

Table 1
Specific surface area, pore size, and pore volume of $Cu_wMn_yTi_{1-y}$-CO_3 LDHs and the corresponding $Cu_wMn_yTi_{1-y}O_x$ LDOs.

Samples	BET SSA (m^2/g)	BJH Pore size (Å)	BJH pore volume (cm^3/g)
$Cu_{0.5}Mn_{0.5}Ti_{0.5}CO_3$ LDH	86.6	46.0	0.199
$Cu_1Mn_{0.5}Ti_{0.5}CO_3$ LDH	113.5	71.8	0.408
$Cu_2Mn_{0.5}Ti_{0.5}CO_3$ LDH	99.8	46.3	0.231
$Cu_3Mn_{0.5}Ti_{0.5}CO_3$ LDH	68.3	45.2	0.154
$Cu_{0.5}Mn_{0.5}Ti_{0.5}O_x$ LDO	67.0	59.0	0.198
$Cu_1Mn_{0.5}Ti_{0.5}O_x$ LDO	102.1	66.3	0.339
$Cu_2Mn_{0.5}Ti_{0.5}O_x$ LDO	83.2	79.6	0.331
$Cu_3Mn_{0.5}Ti_{0.5}O_x$ LDO	56.0	54.7	0.153
Mn/TiO_2	34.3	56.3	0.112
Cu-Mn/TiO_2	45.1	63.6	0.104

3.2. NH_3-SCR activity of $Cu_wMn_yTi_{1-y}O_x$ catalysts

3.2.1. The effect of catalyst components

To further investigate the role of catalyst components in $Cu_wMn_yTi_{1-y}O_x$, catalysts with different molar ratios of Cu/(Mn + Ti) and Mn/Ti were prepared and catalytically evaluated. Fig. 3 presents the influences of Cu/(Mn + Ti) ratio (0.5, 1, 2, and 3) and Mn/Ti ratio (1:3, 1:1, and 3:1) on the De-NO_x activity of $Cu_wMn_yTi_{1-y}O_x$ catalysts in the low temperature range of 100–250 °C. Initially, we optimized the Cu/(Mn + Ti) molar ratio of $Cu_wMn_{0.5}Ti_{0.5}O_x$ by varying the Cu/(Mn + Ti) ratio from 0.5 to 1, 2, and 3. It could be seen that $Cu_1Mn_{0.5}Ti_{0.5}O_x$ represents the best SCR catalyst, with a De-NO_x up to 90% at 200 °C.

The effect of Mn/Ti molar ratio (1:3, 1:1 and 3:1) was also investigated after determining the optimal Cu/(Mn + Ti), as shown in Fig. 3(b). The NO_x conversions increased obviously by increasing the Mn/Ti molar ratio from 1:3 to 1:1 at 100–250 °C. However, the NO_x conversion decreased for a certain extent with a further increase of Mn/Ti ratio from 1:1 to 3:1. For instance, at 100, 150, 200, and 250 °C, the NO_x conversion was decreased from 52.2%, 78.4%, 90%, and 80.8% to 30.9%, 51.1%, 80.8%, and 70.3%, respectively. It is well known that when the loading exceeds the maximum loading of the support monolayer, sintering will occur, thereby resulting in a decrease in the NO_x conversion. These data clearly demonstrated that the Cu/(Mn + Ti) and Mn/Ti molar ratios had a significant influence on the De-NO_x activity of catalysts, and the optimum composition $Cu_1Mn_{0.5}Ti_{0.5}O_x$ exhibited the highest NO_x conversion of 90% at 200 °C.

In the following section, a comparative study on Mn/TiO_2, Cu-Mn/TiO_2, and $Cu_1Mn_{0.5}Ti_{0.5}O_x$ catalysts was performed, as shown in Fig. 4. It can be seen that the performance of Mn/TiO_2 and Cu-Mn/TiO_2 was worse than that of $Cu_1Mn_{0.5}Ti_{0.5}O_x$ catalyst within the whole experimental temperature range. The low temperature activities of Cu-Mn/TiO_2 and $Cu_1Mn_{0.5}Ti_{0.5}O_x$ catalysts, with the introduction of Cu, were significantly better than that of Mn/TiO_2 catalyst. For Mn/TiO_2, Cu-Mn/TiO_2, and $Cu_1Mn_{0.5}Ti_{0.5}O_x$, the NO_x conversion at 200 °C was 80.7%, 86.1%, and 90%, respectively. It is apparent that the $Cu_1Mn_{0.5}Ti_{0.5}O_x$ catalyst possessed much better SCR performance than the other two catalysts. In addition, the selectivity of NO_x conversion into N_2 was also investigated over Mn/TiO_2, Cu-Mn/TiO_2, and $Cu_1Mn_{0.5}Ti_{0.5}O_x$ catalysts, as shown in Fig. 4(a). The N_2 selectivity of $Cu_1Mn_{0.5}Ti_{0.5}O_x$ was 99.4%, which is much higher than that of Cu-Mn/TiO_2 (95%) and Mn/TiO_2 (88%) at 200 °C. Thus, it can be concluded that the $Cu_1Mn_{0.5}Ti_{0.5}O_x$ catalyst not only possesses high De-NO_x

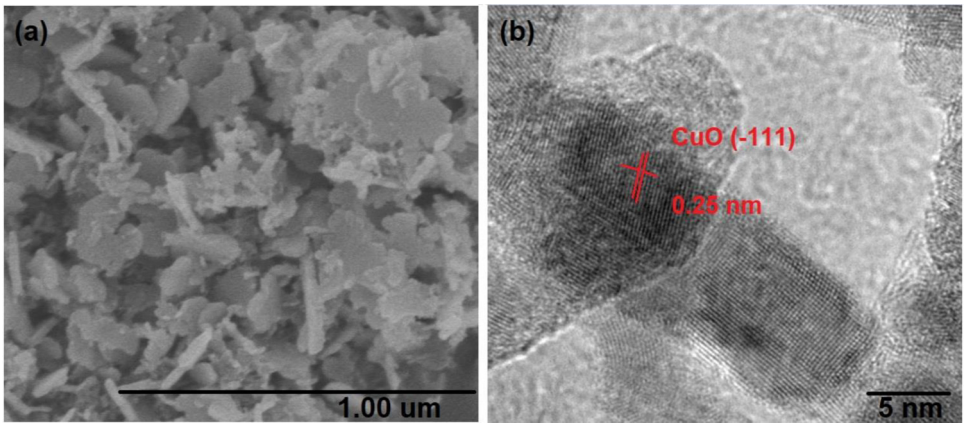

Fig. 2. (a) SEM image of $Cu_1Mn_{0.5}Ti_{0.5}$-CO_3 LDH, and (b) the HR-TEM image of $Cu_1Mn_{0.5}Ti_{0.5}O_x$ calcined at 400 °C.

property, but also has high N_2 selectivity.

More control catalysts with higher Cu and Mn loadings, 20 wt% Cu-20 wt% Mn/TiO_2 and 40 wt% Cu-20 wt% Mn/TiO_2, were also synthesized and evaluated. As shown in Fig. S2, the NO_x conversion decreased with increasing the loadings of Cu and Mn, which was 86.1%, 80.2%, and 60.3% for 10 wt% Cu-10 wt% Mn/TiO_2, 20 wt% Cu-20 wt% Mn/TiO_2, and 40 wt% Cu-20 wt% Mn/TiO_2, respectively. This is due to the maximum monolayer load limitation of the carrier. However, $Cu_1Mn_{0.5}Ti_{0.5}O_x$ showed higher NO_x conversion of 90% under the same condition. These results demonstrated that the catalysts obtained by calcination of LDHs can avoid the maximum monolayer load limitation of the carrier, and thereby obtaining highly dispersed catalysts with improved catalytic activity.

To clarify why $Cu_1Mn_{0.5}Ti_{0.5}O_x$ catalyst has better activity than conventional catalysts, the XRD patterns of samples were analyzed and displayed in Fig. 4(b). After 400 °C calcination, both Mn/TiO_2 and Cu-Mn/TiO_2 were converted into a mixture of oxides and spinels. For Mn/TiO_2, the diffraction peaks can be attributed to anatase TiO_2 and crystallized MnO_2 (JCPDS No. 24-0735). For Cu-Mn/TiO_2, there were some new peaks corresponded to CuO phase (JCPDS No. 48-1548). For $Cu_1Mn_{0.5}Ti_{0.5}O_x$, only CuO phase (JCPDS No. 48-1548) was observed, while the MnO_x phase was not identified. It implies that the manganese oxides might be in a highly dispersed state.

In order to identify the chemical composition and the state of surface species of different catalysts, the samples were examined using XPS analyses. The photoelectron spectra of O 1 s, Cu 2p, and Mn 2p of Mn/TiO_2, $Cu_1Mn_{0.5}Ti_{0.5}O_x$, and Cu-Mn/TiO_2 samples were displayed in Fig. 5. The XPS spectra of Cu 2p for $Cu_1Mn_{0.5}Ti_{0.5}O_x$ and Cu-Mn/TiO_2 catalysts were displayed in Fig. 5(a). For these two catalysts, the Cu 2p3/2 and Cu 2p1/2 peaks at 934 and 955.0 eV were observed, with two satellite peaks at 960.0–965.0 eV and 938.0–945.0 eV, respectively. The value of $Cu^{2+}/(Cu^{2+}+Cu^{1+})$ in $Cu_1Mn_{0.5}Ti_{0.5}O_x$ (63%) is higher than that in Cu-Mn/TiO_2 (49.4%), which is beneficial for promoting the low-temperature SCR activity.

The XPS spectra of Mn 2p for Mn/TiO_2, Cu-Mn/TiO_2, and $Cu_1Mn_{0.5}Ti_{0.5}O_x$ catalysts were displayed in Fig. 5(b), which suggests that MnO_x existed as a mixed-valence state in these three catalysts. The value of $Mn^{4+}/(Mn^{4+}+Mn^{3+})$ follows the order of $Cu_1Mn_{0.5}Ti_{0.5}O_x$ (53.4%) > Cu-Mn/TiO_2 (48.6%) > Mn/TiO_2 (38.0%). Previous studies have demonstrated that the presence of Mn^{4+} species is conducive to the low temperature De-NO_x activity [25,33–35]. Therefore, the higher value of $Mn^{4+}/(Mn^{4+}+Mn^{3+})$ in $Cu_1Mn_{0.5}Ti_{0.5}O_x$ catalyst may be one of the reasons for its higher catalytic activity at low temperature.

In Fig. 5(c), all Ti 2p XPS spectra consist two peaks at 464.3 and 458.3 eV, which represent Ti 2p1/2 and Ti 2p3/2. The result also indicated that Ti^{4+} state is the main valence in all catalysts [36,37]. After introducing Cu, the binding energies shifted to lower values. This indicated that the introduction of Cu can influence the chemical environments of Ti^{4+} in Cu-Mn/TiO_2 and $Cu_1Mn_{0.5}Ti_{0.5}O_x$ catalysts.

The O 1 s XPS spectra of $Cu_1Mn_{0.5}Ti_{0.5}O_x$, Cu-Mn/TiO_2, and Mn/TiO_2 catalysts were displayed in Fig. 5(d), which could be fitted into two peaks. The peak at 528.7–530.9 eV corresponds to lattice oxygen (O_α), whereas the other peak at 531.4–532.5 eV is related to the surface adsorbed oxygen (O_β) [38]. It has been reported that O_β has an important influence on the oxidation reaction due to its higher mobility [39–41]. The $O_\beta/(O_\alpha+O_\beta)$ ratios of Cu-Mn/TiO_2, and Mn/TiO_2 catalysts were significantly lower than that of $Cu_1Mn_{0.5}Ti_{0.5}O_x$ sample. XPS results indicated that the relatively higher ratios of $Cu^{2+}/(Cu^{2+}+Cu^{1+})$, $Mn^{4+}/(Mn^{4+}+Mn^{3+})$, and $O_\beta/(O_\alpha+O_\beta)$ might account for the good De-NO_x performance of $Cu_1Mn_{0.5}Ti_{0.5}O_x$ catalyst.

The FTIR spectroscopy of pyridine chemisorption is most widely used to detect the surface acidity of catalysts. Fig. 6(a) shows the FTIR spectra of pyridine adsorbed on Mn/TiO_2, $Cu_1Mn_{0.5}Ti_{0.5}O_x$, and Cu-Mn/TiO_2. The bands at about 1446, 1490, 1577, and 1597 cm^{-1} can be attributed to the pyridine coordinated to L acids, whereas the characteristic band at 1546 cm^{-1} corresponds to B acid sites [42]. The

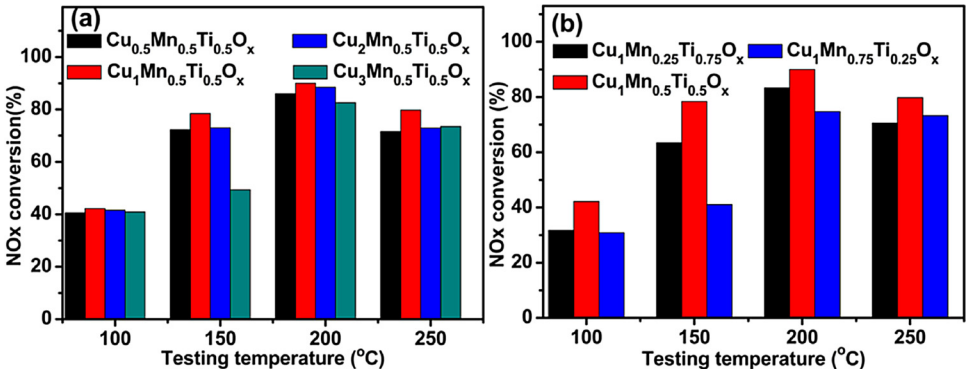

Fig. 3. The influence of (a) Cu/(Mn + Ti) ratio (0.5, 1, 2, and 3), (b) Mn/Ti ratio (1:3, 1:1, and 3:1) on the activity of $Cu_wMn_yTi_{1-y}O_x$ mixed oxide catalysts. Calcination temperature = 400 °C, and operating temperature = 100, 150, 200, and 250 °C. Reaction conditions: $[NO_x]$ = $[NH_3]$ = 500 ppm, $[O_2]$ = 5%, balance Ar, total flow rate = 200 mL/min, catalyst 0.15 g.

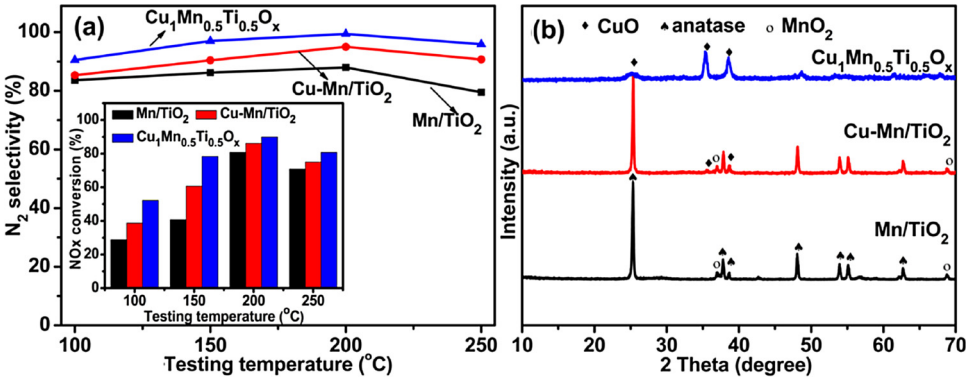

Fig. 4. (a) The NO_x conversion and N_2 selectivity over Mn/TiO_2, Cu-Mn/TiO_2, and $Cu_1Mn_{0.5}Ti_{0.5}O_x$ catalysts, and (d) The XRD patterns of $Cu_1Mn_{0.5}Ti_{0.5}O_x$, Cu-Mn/TiO_2, and Mn/TiO_2 calcined at 400 °C. Reaction conditions: [NO_x] = [NH_3] = 500 ppm, [O_2] = 5%, balance Ar, total flow rate = 200 mL/min, catalyst 0.15 g.

concentrations of the L and B sites can be quantified from the intensities of the peaks at about 1450 and 1546 cm^{-1}, which follows the order of $Cu_1Mn_{0.5}Ti_{0.5}O_x$ (230.5 μmol/g) > Cu-Mn/TiO_2 (127.2 μmol/g) > Mn/TiO_2 (102.1 μmol/g) [43,44]. Fig. 6(b) shows the relationship between the catalytic performance and acidity. Obviously, with the introduction of Cu, the catalytic performance of $Cu_1Mn_{0.5}Ti_{0.5}O_x$ catalyst increases with elevating the quantities of L and B acids.

The surface acidity and surface Cu and Mn active species of Mn/TiO_2, Cu-Mn/TiO_2, and CuMnTiO_x catalysts were investigated by NH_3-TPD and H_2-TPR experiments, as shown in Fig. 6(c, d). Since the adsorption of NH_3 is very important in NH_3-SCR reaction, NH_3-TPD analysis was used to determine the catalyst surface acidity. Two desorption peaks for all samples were observed, which can be described as the reduction of MnO_x and/or copper species. The desorption peak at low temperature located at about 155 °C. The amounts of desorbed NH_3 (surface acidity) were compared by integrating the NH_3-TPD curves and it is obvious that $Cu_1Mn_{0.5}Ti_{0.5}O_x$ possesses much higher intensity than that of Mn/TiO_2 and Cu-Mn/TiO_2, indicating $Cu_1Mn_{0.5}Ti_{0.5}O_x$ has more acidic sites for NH_3 adsorption. The reaction mechanism of NH_3-SCR has been previously investigated and it has been demonstrated that the catalytic property is related to the surface acidity of catalysts [45].

According to literature report, the reduction peak of Mn/TiO_2 catalyst between 150 and 500 °C could be divided into three steps: MnO_2 → Mn_2O_3 → Mn_3O_4 → MnO [46]. For Cu-Mn/TiO_2, $Cu_{0.5}Mn_{0.5}Ti_{0.5}O_x$, $Cu_1Mn_{0.5}Ti_{0.5}O_x$, $Cu_2Mn_{0.5}Ti_{0.5}O_x$, and $Cu_3Mn_{0.5}Ti_{0.5}O_x$ samples, three reduction peaks were observed, which related to the stepwise reduction of CuO_x species i.e., Cu^{2+} → Cu^{1+} (about 136 °C) and Cu^{1+}→Cu (about 163 °C) [47], and the bulk Cu^{2+} reduction [48], overlapped with the reduction of surface MnO_x species. For Cu-Mn/TiO_2, in addition to the reduction peak at about 250 °C, actually there was one peak at around 146 °C for the reduction of Cu. However, because the peak was so weak that after being combined with other data, this peak became not so obvious. In order to prevent any misleading, we provided the H_2-TPR profile of Cu-Mn/TiO_2 catalyst separately as Fig. S1.

For $Cu_1Mn_{0.5}Ti_{0.5}O_x$, the intensity of H_2-TPR at low temperature was stronger than that of Cu-Mn/TiO_2 and Mn/TiO_2, suggesting that

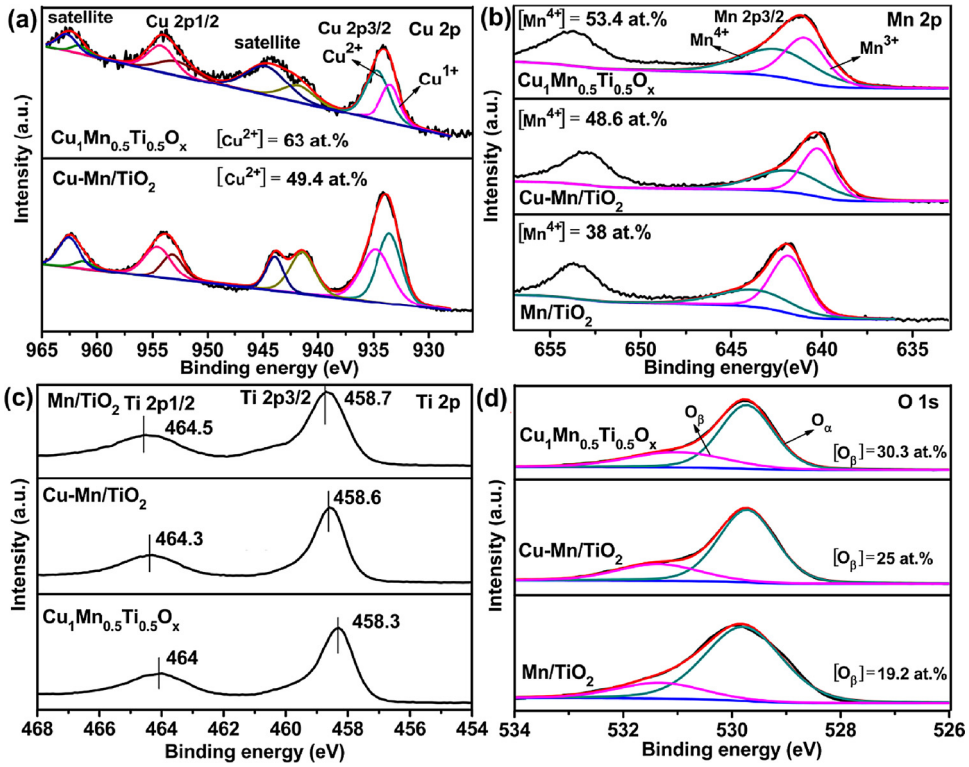

Fig. 5. XPS spectra of (a) Cu 2p, (b) Mn 2p, (c) Ti 2p, and (d) O 1 s of $Cu_1Mn_{0.5}Ti_{0.5}O_x$, Cu-Mn/TiO_2, and Mn/TiO_2 catalysts.

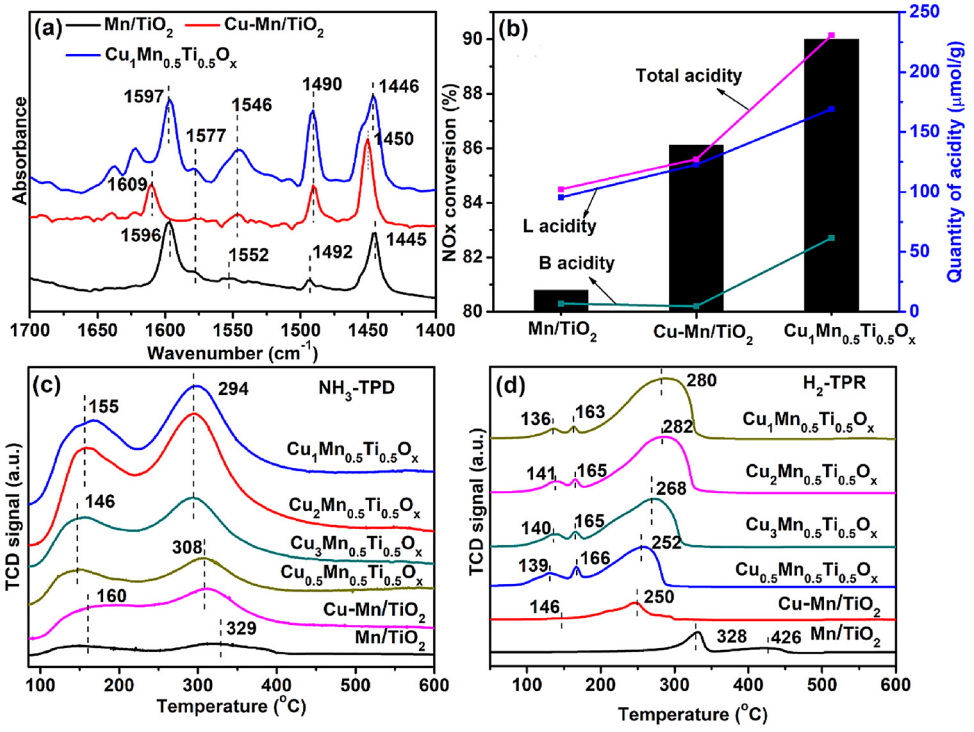

Fig. 6. (a) FTIR spectra of pyridine adsorbed at 200 °C on $Cu_1Mn_{0.5}Ti_{0.5}O_x$, Cu-Mn/TiO_2, and Mn/TiO_2 catalysts, (b) Variations in the quantity of acidity and the catalytic performance of $Cu_1Mn_{0.5}Ti_{0.5}O_x$, Cu-Mn/TiO_2, and Mn/TiO_2 catalysts at 200 °C, (c) NH_3-TPD and (d) H_2-TPR profiles over the Mn/TiO_2, Cu-Mn/TiO_2, $Cu_{0.5}Mn_{0.5}Ti_{0.5}O_x$, $Cu_1Mn_{0.5}Ti_{0.5}O_x$, $Cu_2Mn_{0.5}Ti_{0.5}O_x$, and $Cu_3Mn_{0.5}Ti_{0.5}O_x$ catalysts.

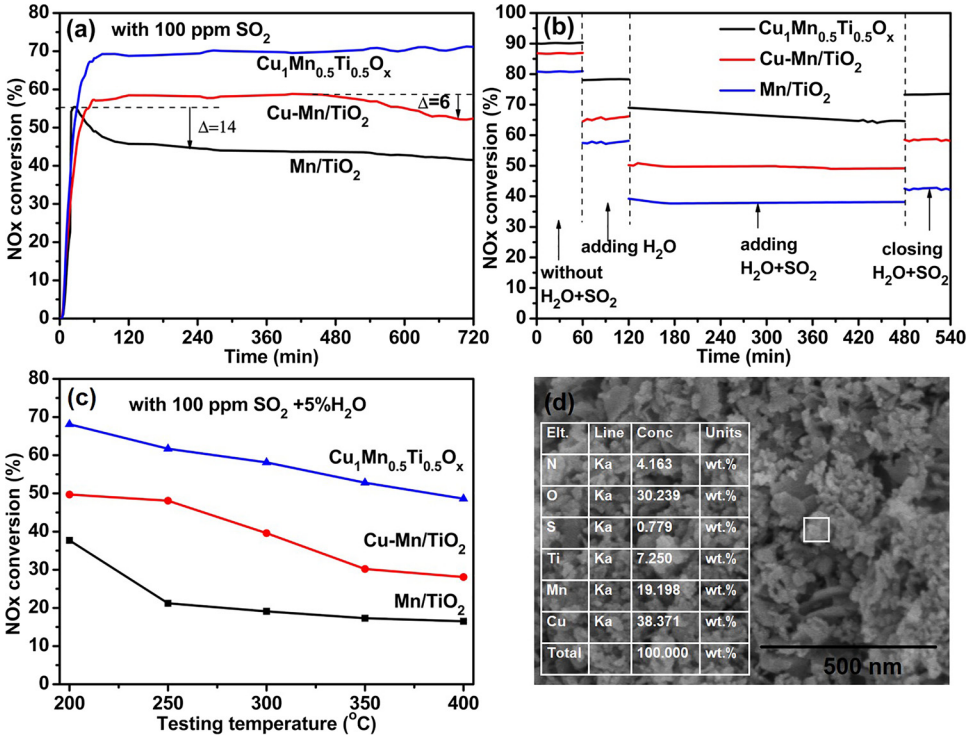

Fig. 7. (a) Long-term isothermal NO_x conversion of catalysts in the presence of 100 ppm SO_2 at 200 °C, (b) The influence of 5% H_2O and 100 ppm SO_2 addition on the NO_x conversion of catalysts at 200 °C, (c) The influence of 5% H_2O and 100 ppm SO_2 on the NO_x conversion of catalysts at different temperature, and (d) SEM image of $Cu_1Mn_{0.5}Ti_{0.5}O_x$ after used in the gas containing 5% H_2O and 100 ppm SO_2 at 200 °C. The inset Table is the SEM-EDX analysis of the selected area of sample. Reaction conditions: $[NO_x]$ = $[NH_3]$ = 500 ppm, $[O_2]$ = 5%, $[H_2O]$ = 5%, $[SO_2]$ = 100 ppm, balance Ar, total flow rate = 200 mL/min, catalyst 0.15 g.

$Cu_1Mn_{0.5}Ti_{0.5}O_x$ surface possesses more highly dispersed copper and manganese oxide crystallites, which are important active species for the low-temperature SCR reaction. Therefore, the increase of surface active species on $Cu_1Mn_{0.5}Ti_{0.5}O_x$ maybe one reason for its higher NO_x conversion than the conventional Mn/TiO_2 catalyst. The H_2-TPR peak areas of Cu-Mn/TiO_2 and $CuMnTiO_x$ are larger than that of Mn/TiO_2. The H_2 consumptions of samples were quantified through a pulse experiment, which followed the sequence of $Cu_1Mn_{0.5}Ti_{0.5}O_x$ (1.15 mmol/g) > $Cu_2Mn_{0.5}Ti_{0.5}O_x$ (0.82 mmol/g) > $Cu_3Mn_{0.5}Ti_{0.5}O_x$ (0.69 mmol/g) > $Cu_{0.5}Mn_{0.5}Ti_{0.5}O_x$ (0.47 mmol/g) > Cu-Mn/TiO_2 (0.25 mmol/g) > Mn/TiO_2 (0.16 mmol/g). The improvement maybe attributed to the synergistic influence between copper and manganese species. Therefore, $Cu_1Mn_{0.5}Ti_{0.5}O_x$ prepared by LDH calcination has higher Mn and Cu species reduction ability, which means that the surface oxygen mobility increases and the SCR reaction proceeds rapidly [20,49].

3.2.2. The effect of SO_2 and H_2O

SO_2 poisoning is a critical problem for SCR catalysts. As shown in Fig. 7(a), the long-term De-NO_x properties of Mn/TiO_2, Cu-Mn/TiO_2, and $Cu_1Mn_{0.5}Ti_{0.5}O_x$ catalysts were evaluated at 200 °C with 100 ppm

Table 2
Specific surface area, pore size, and pore volume of fresh and sulfated $Cu_1Mn_{0.5}Ti_{0.5}O_x$, Cu-Mn/TiO_2, and Mn/TiO_2.

Samples	BET SSA (m^2/g)	BJH Pore size (Å)	BJH pore volume (cm^3/g)
$Cu_1Mn_{0.5}Ti_{0.5}O_x$	102.1	66.3	0.339
Cu-Mn/TiO_2	45.1	63.6	0.104
Mn/TiO_2	34.3	56.3	0.112
$Cu_1Mn_{0.5}Ti_{0.5}O_x$-S	69.3	49.8	0.173
Cu-Mn/TiO_2-S	26.4	139.8	0.115
Mn/TiO_2-S	16.4	127.7	0.104

SO_2. For $Cu_1Mn_{0.5}Ti_{0.5}O_x$ sample, the NO_x conversion only slightly decreased even after running for 12 h. However, the decreases in NO_x conversion for Mn/TiO_2 and Cu-Mn/TiO_2 were significant, which was 14% and 6% respectively after 10 h. These results clearly demonstrated that $Cu_1Mn_{0.5}Ti_{0.5}O_x$ sample is much less effected by SO_2 than Mn/TiO_2 and has great potential for practical applications.

For low-temperature NH_3-SCR, the influences of H_2O and SO_2 on the De-NO_x performance can not be ignored [50,51]. Thus, the resistance of Mn/TiO_2, Cu-Mn/TiO_2, and $Cu_1Mn_{0.5}Ti_{0.5}O_x$ catalysts to both H_2O and SO_2 was also investigated at 200 °C, as displayed in Fig. 7(b). Without H_2O and SO_2, the NO_x conversion for Mn/TiO_2, Cu-Mn/TiO_2, and $Cu_1Mn_{0.5}Ti_{0.5}O_x$ was 80%, 86%, and 90%, respectively. After adding 5% H_2O, the NO_x conversion of Mn/TiO_2, Cu-Mn/TiO_2, and $Cu_1Mn_{0.5}Ti_{0.5}O_x$ decreased to 58%, 66.1% and 78.3%, respectively. After adding 5% H_2O and 100 ppm SO_2 simultaneously, the synergistic influence of H_2O and SO_2 further decreased the catalysts property. However, $Cu_1Mn_{0.5}Ti_{0.5}O_x$ still resulted in higher activity than Mn/TiO_2 and Cu-Mn/TiO_2, even with both H_2O and SO_2. For $Cu_1Mn_{0.5}Ti_{0.5}O_x$, the NO_x conversion was still 64.6% after 6 h, which is much higher than that for Mn/TiO_2 (38.0%) and Cu-Mn/TiO_2 (49.1%). Once H_2O and SO_2 were stopped, the NO_x conversion for $Cu_1Mn_{0.5}Ti_{0.5}O_x$ recovered to 73.4%, and the conversion of Mn/TiO_2 and Cu-Mn/TiO_2 was only recovered to 42.1% and 58.1%, respectively. This results indicated that $Cu_1Mn_{0.5}Ti_{0.5}O_x$ catalyst also possesses better resistance to the coexistence of SO_2 and H_2O than Mn/TiO_2 and Cu-Mn/TiO_2 catalysts.

In order to observe the viability of catalysts, the effect of 100 ppm SO_2 and 5% H_2O at higher temperatures (200–400 °C) of $Cu_1Mn_{0.5}Ti_{0.5}O_x$, Cu-Mn/TiO_2, and Mn/TiO_2 catalysts were comparatively examined, as shown the Fig. 7(c). With the increase of testing temperature, the catalytic property of all catalysts showed a certain degree of decline. $Cu_1Mn_{0.5}Ti_{0.5}O_x$ catalyst showed higher catalytic property in the whole tested temperature range. For instance, at 250 °C, $Cu_1Mn_{0.5}Ti_{0.5}O_x$ resulted in a NO_x conversion of 61.7%, which is much higher than that for Cu-Mn/TiO_2 (48.1%) and Mn/TiO_2 (21.2%). At 400 °C, the NO_x conversion of $Cu_1Mn_{0.5}Ti_{0.5}O_x$ decreased to 48.6%, but it was still higher than that of Cu-Mn/TiO_2 (28.1%) and Mn/TiO_2

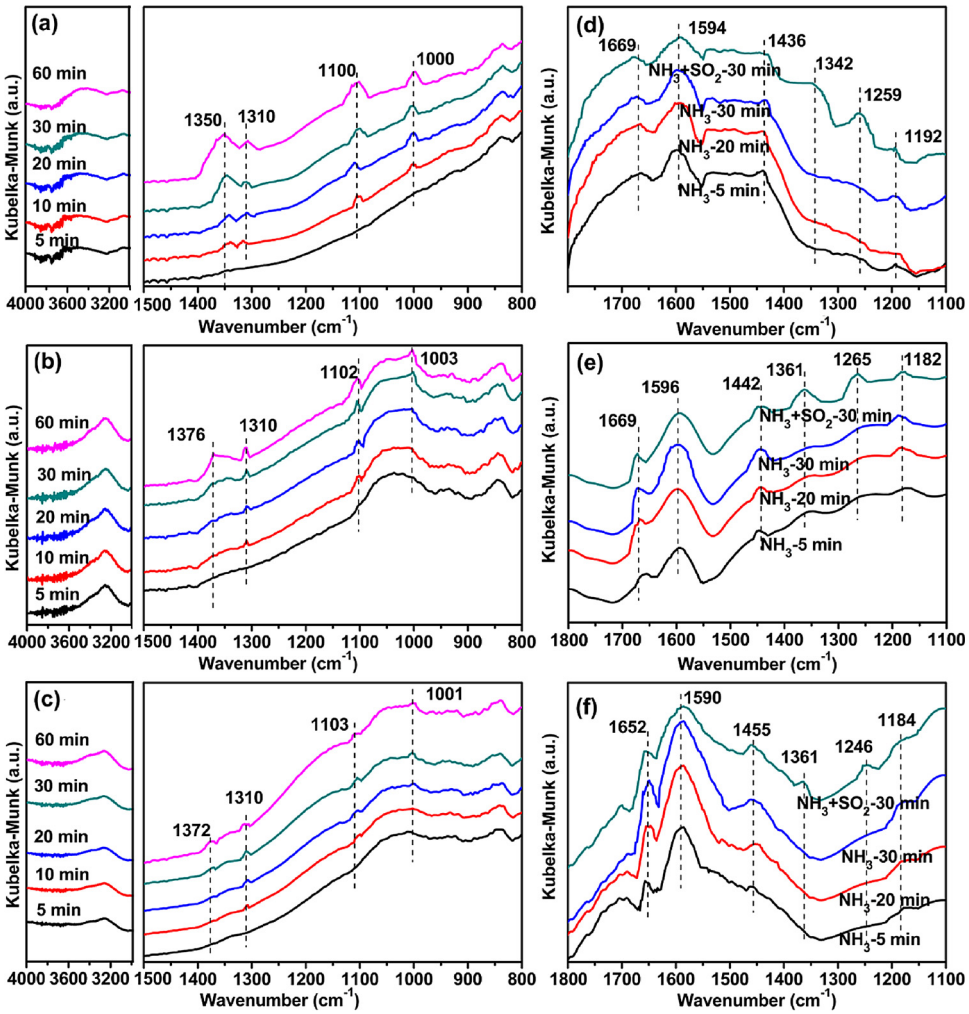

Fig. 8. In situ DRIFT 500 ppm SO_2 + 5% O_2 co-adsorption spectra over (a) Mn/TiO_2 (b) Cu-Mn/TiO_2, and (c) $Cu_1Mn_{0.5}Ti_{0.5}O_x$ catalysts at 200 °C as a function of time for 60 min. In situ DRIFT spectra obtained after a 30 min exposure to 1000 ppm NH_3 and 1000 ppm NH_3 + 500 ppm SO_2 in the presence of 5% O_2 over (d) Mn/TiO_2, (e) Cu-Mn/TiO_2, and (f) $Cu_1Mn_{0.5}Ti_{0.5}O_x$ catalysts at 200 °C.

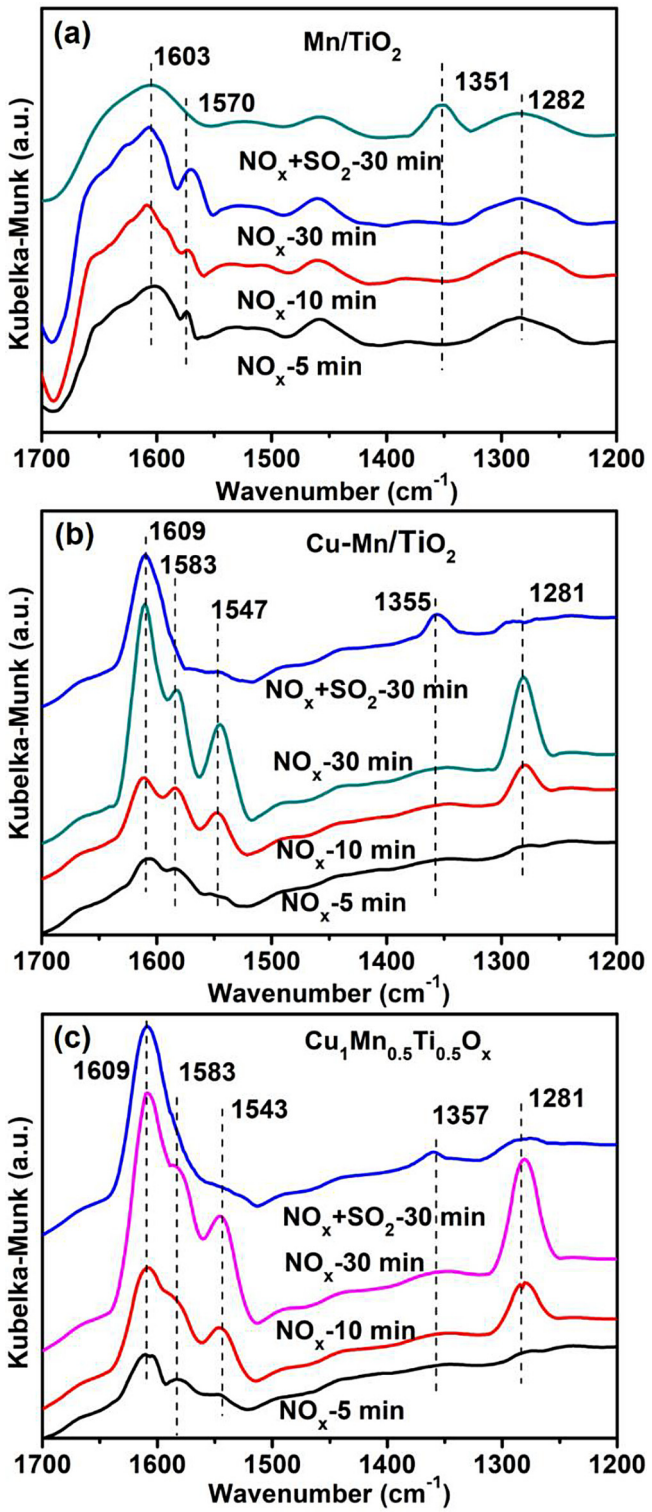

Fig. 9. In situ DRIFT spectra obtained after a 30 min exposure to 2000 ppm NO + 5% O_2 or 2000 ppm NO + 500 ppm SO_2 in the presence of 5% O_2 over (a) Mn/TiO_2, (b) $Cu\text{-}Mn/TiO_2$, and (c) $Cu_1Mn_{0.5}Ti_{0.5}O_x$ catalysts at 200 °C.

(16.5%). In all, the results suggested that $Cu_1Mn_{0.5}Ti_{0.5}O_x$ has better viability and stability, even at higher temperatures and in the presence of SO_2 and H_2O.

The used catalysts were further characterized using XRD and SEM analyses. In the XRD patterns of Fig. S3, no characteristic diffraction peak of the sulfate species was found. This may be due to the short time of SO_2 poisoning and the low content of sulfate species. We then examined the morphology of the used $Cu_1Mn_{0.5}Ti_{0.5}O_x$ by SEM characterization, as shown in Fig. 7(d). Some deposits could be seen on the surface, which may be attributed to the formation of $(NH_4)_2SO_4$/NH_4HSO_4 and sulfate species. To further confirm the existence of sulfate species, SEM–EDS analysis was performed as shown in the inset of Fig. 7(d), which indicated that the sulfate species indeed existed on the surface of catalyst, although the amount was quite small.

In addition, the SSA of fresh and deactivated catalysts are summarized in Table 2. The SSA of fresh $Cu_1Mn_{0.5}Ti_{0.5}O_x$, $Cu\text{-}Mn/TiO_2$, and Mn/TiO_2 was 102.1, 45.1, and 34.3 m^2/g, respectively. After the sulfate species formed and deposited on the catalysts surface, the SSA of all sulfated $Cu_1Mn_{0.5}Ti_{0.5}O_x$, $Cu\text{-}Mn/TiO_2$, and Mn/TiO_2 became 69.3, 26.4, and 16.4 m^2/g, respectively. Obviously, the SSA of all samples decreased to a certain extent, which may be one reason to explain the decrease in catalytic activity. However, it is apparent that $Cu_1Mn_{0.5}Ti_{0.5}O_x$ also possesses larger SSA than other catalysts. The BET analyses also confirmed that the $Cu_1Mn_{0.5}Ti_{0.5}O_x$ catalyst has stronger resistance to SO_2 than the other controlled catalysts.

The DRIFT experiment of SO_2 + O_2 at 200 °C was used to understand the inter-relationship between catalysts and sulfates. As displayed in Fig. 8, the symmetric stretching frequencies of O—S—O species at about 1000 and 1100 cm^{-1}, and the asymmetric stretching frequencies of O═S═O species at about 1310 and 1350 cm^{-1} were detected [49,52,53]. However, the band at 1350 cm^{-1} on Mn/TiO_2 was much stronger than that on $Cu_1Mn_{0.5}Ti_{0.5}O_x$, indicating that much more sulfates species was formed on Mn/TiO_2. The results showed that the formation of sulfate species is due to sulfation at 200 °C, while $Cu_1Mn_{0.5}Ti_{0.5}O_x$ has better resistance to SO_2 than Mn/TiO_2.

NH_3 adsorption is believed to be an important step in NH_3-SCR reaction. Therefore in order to clarify how SO_2 might impact this process, a comparative study was performed. Fig. 8(d–f) displays the DRIFT spectra of $Cu\text{-}Mn/TiO_2$, $Cu_1Mn_{0.5}Ti_{0.5}O_x$, and Mn/TiO_2 after exposure to NH_3/N_2 and SO_2 co-adsorption with NH_3 at different times. The bands at 1590–1596 cm^{-1} and 1182–1192 cm^{-1} belong to NH_3 coordinated to L acids [52,54]. The bands at 1652–1669 cm^{-1} and 1436–1455 cm^{-1} assigned to B acids [55]. However, for $Cu_1Mn_{0.5}Ti_{0.5}O_x$, the intensity of band at 1590 and 1652 cm^{-1} was much stronger than that on other catalysts, indicating a stronger adsorption of NH_3 due to the addition of Cu. This NH_3-DRIFT conclusion is consistent with the pyridine infrared and NH_3-TPD conclusions, suggesting that $Cu_1Mn_{0.5}Ti_{0.5}O_x$ has more L and B acid sites, and may be one of the reasons for its high activity.

All catalysts were then exposed to both NH_3 and SO_2 for 30 min. Compared with only NH_3 exposure, the intensity of bands corresponding to NH_3 on L acid sites (about 1590 cm^{-1}) and B acid sites (1652 cm^{-1}) slightly decreased, which indicated that the amount of adsorbed NH_3 on L and B acid sites was reduced. However, the emergence of new bands at 1342–1361 cm^{-1} and 1246–1265 cm^{-1} suggested the formation of O═S═O and HSO_4^- species, respectively [49]. These results showed that SO_2 indeed has an impact on NH_3 adsorption, and forms some new NH_4HSO_4 species. Notably, it is clear that during SO_2 co-adsorption with NH_3, $Cu_1Mn_{0.5}Ti_{0.5}O_x$ still has more L acid sites and less NH_4HSO_4 species compared with other catalysts, which is very important for the occurrence of SCR reactions.

In order to better explain the formation of NO_2 in the mechanism scheme, an NO + O_2 adsorption experiment on in situ DRIFT was performed. For the NO + O_2 adsorption experiments, 2000 ppm NO + 5% O_2 was injected for 30 min at 200 °C and the corresponding spectra were recorded as a function of time. As shown in Fig. 9, the formation of bands at about 1609, 1583, 1543, and 1281 cm^{-1} were observed after NO + O_2 adsorption on all samples. Based on literature studies, the two bands at about 1583 and 1281 cm^{-1} were assigned to nitrate species, while the band at about 1609 cm^{-1} was attributed to adsorbed NO_2 species [56–58], and the band at 1543 cm^{-1} could also be assigned to NO_2- containing species, like nitrito (O-bound NO_2) and nitrato (NO_3) species [59].

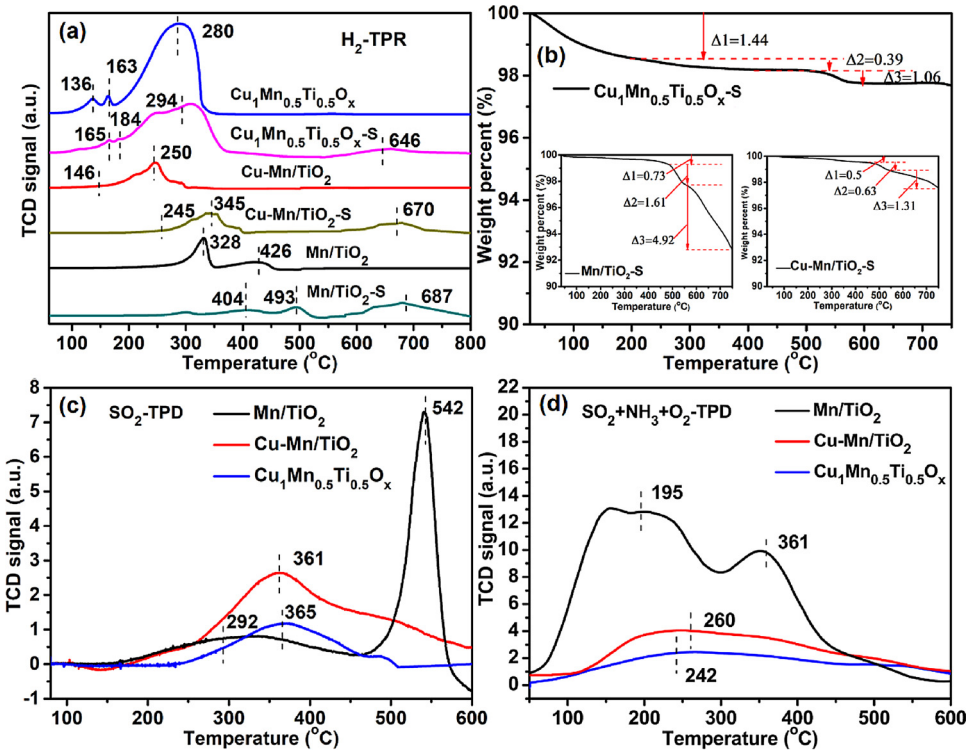

Fig. 10. (a) H_2-TPR of fresh and pre-sulfated Mn/TiO_2, $Cu\text{-}Mn/TiO_2$, and $Cu_1Mn_{0.5}Ti_{0.5}O_x$ catalysts, (b) TGA curve of pre-sulfated Mn/TiO_2, $Cu\text{-}Mn/TiO_2$, and $Cu_1Mn_{0.5}Ti_{0.5}O_x$ catalysts, (c) SO_2-TPD of Mn/TiO_2, $Cu\text{-}Mn/TiO_2$, and $Cu_1Mn_{0.5}Ti_{0.5}O_x$ catalysts, and (d) $SO_2 + O_2 + NH_3$-TPD of Mn/TiO_2, $Cu\text{-}Mn/TiO_2$, and $Cu_1Mn_{0.5}Ti_{0.5}O_x$ catalysts.

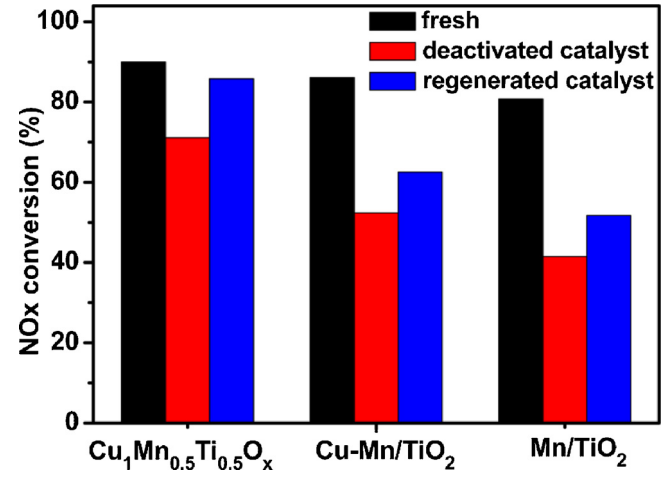

Fig. 11. NO_x conversions of fresh, deactivated and regenerated catalysts treated by thermal regeneration. Reaction conditions: $[NO_x] = [NH_3] = 500$ ppm, $[O_2] = 5\%$, $[H_2O] = 5\%$, $[SO_2] = 100$ ppm, balance Ar, total flow rate = 200 mL/min, GHSV = 60,000 h^{-1}, testing temperature = 200 °C, catalyst 0.15 g.

The enhancement role of copper oxide can be interpreted that NO could be oxidized to NO_2 easily at low temperatures. To better explain the formation of NO_2 in the mechanism scheme, NO oxidation experiment was conducted. The inlet gas contained 500 ppm NO_x (about 455 ppm NO, and 45 ppm NO_2), and 5% O_2 with Ar as balance. At 200 °C, the $Cu_1Mn_{0.5}Ti_{0.5}O_x$ was exposed to the gas for 140 min, the concentration of each component was monitored. Fig. S4 shows that the concentration of NO_2 increased from 45 ppm to 152 ppm, indicating that NO was oxidized to NO_2 in the presence of catalyst. This is conducive to the formation of ammonium nitrite, which promotes the occurrence of "fast-SCR".

In addition, the interactions between SO_2 and NO_x were also investigated by comparing the in situ DRIFT spectra taken during catalyst exposure to NO_x and SO_2 co-adsorption with NO_x, as shown in Fig. 9. After adding SO_2, most of the bands for NO_x species except the one at about 1609 cm^{-1} disappeared, and in the meantime, the new band at 1351–1357 cm^{-1} belongs to the asymmetric stretching frequencies of O═S═O species was observed. The results again proved that SO_2 competes with NO_x for surface adsorption sites, resulting in less NO_x adsorption. It is also worth noting that the intensity of sulfur species band on $Cu_1Mn_{0.5}Ti_{0.5}O_x$ was much weaker than that on $Cu\text{-}Mn/TiO_2$ and Mn/TiO_2, and in contrary the intensity of the NO_x species band on $Cu_1Mn_{0.5}Ti_{0.5}O_x$ was stronger than that on $Cu\text{-}Mn/TiO_2$ and Mn/TiO_2. This data further demonstrated that the $Cu_1Mn_{0.5}Ti_{0.5}O_x$ catalyst has better resistance to SO_2 than other catalysts.

In order to study the influence of SO_2 on the redox property of catalysts, the pre-sulfated and fresh catalysts were analyzed by H_2-TPR. As displayed in Fig. 10(a), the reduction peaks of pre-sulfated catalysts shifted to higher temperatures than the fresh catalysts. It has been recommended that the reduction peak temperature is an indication of reducibility, and the lower reduction temperature represents greater reducibility. In addition, the reduction peak area of all the samples reduced, indicating that SO_2 had negative effect on the reducibility of catalysts. For Mn/TiO_2 catalyst, the two reduction peaks located at 328 and 426 °C were greatly shifted to 404 and 493 °C. These data suggested that the addition of Cu can promote the SO_2 resistance of Mn-based SCR catalyst. For the $Cu_1Mn_{0.5}Ti_{0.5}O_x$ catalysts obtained from LDHs precursors, the reduction peak temperatures were still very low even after SO_2 pre-sulfation, which only slightly increased from 136, 163, and 280 °C to 165, 184, and 294 °C. Compared with Mn/TiO_2 and $Cu\text{-}Mn/TiO_2$, the reduction peak for $Cu_1Mn_{0.5}Ti_{0.5}O_x$ was somehow stronger and the peak temperature was still very low.

In addition, a high temperature H_2 consumption peak at 646–687 °C was observed for all pre-sulfated Mn/TiO_2, $Cu\text{-}Mn/TiO_2$, and $Cu_1Mn_{0.5}Ti_{0.5}O_x$ catalysts. This peak was absent with all fresh catalysts, confirming that it was due to the reduction of sulfates species. The TCD signal at high temperature (646–687 °C) assigned to SO_2 and H_2S further supported that sulfur is mainly stored as either sulfates or surface SO_2 groups, consistent with literature reports by Zhang et al. [57] and Wijayanti et al. [60]. The H_2 consumption of Mn/TiO_2-S, $Cu\text{-}Mn/TiO_2$-S, and $Cu_1Mn_{0.5}Ti_{0.5}O_x$-S were also quantified, which followed the

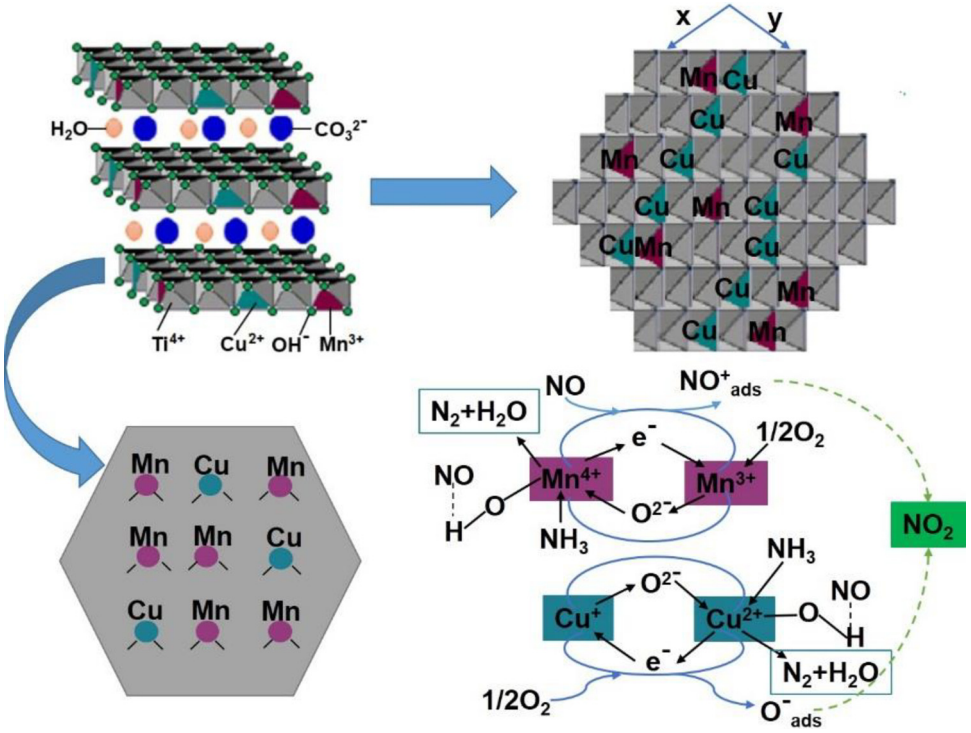

Fig. 12. Schematic illustration of the preparation process of $CuMnTiO_x$, and a redox catalytic cycle of the low-temperature NH_3-SCR reactions over $CuMnTiO_x$ catalysts.

order of $Cu_1Mn_{0.5}Ti_{0.5}O_x$-S (0.81 mmol/g) > Cu-Mn/TiO_2-S (0.16 mmol/g) > Mn/TiO_2-S (0.1 mmol/g). Thus, it can be concluded that $Cu_1Mn_{0.5}Ti_{0.5}O_x$ catalyst has the best SO_2 resistance among all studied catalysts.

To explain this, TGA test was used to analyze the thermal stability of pre-sulfated $Cu_1Mn_{0.5}Ti_{0.5}O_x$, Cu-Mn/TiO_2 and Mn/TiO_2. Fig. 10(b) shows that the weight loss of the pre-sulfated samples was in three steps. The step 1 (26–200 °C) is mainly due to the desorption of water adsorbed on samples [49,61]. The weight loss in step 2 (200–550 °C) was due to the decomposition of $(NH_4)_2SO_4$ and/or NH_4HSO_4 [31], and the weight loss in step 3 (550–800 °C) corresponds to $Ti(SO_4)_2$, $Mn(SO_4)_2$, and/or $CuSO_4$. For the pre-sulfated Mn/TiO_2, it showed a weight loss of 1.61 wt% and 4.92 wt% in step 2 and step 3, respectively. After adding Cu to the Mn-based catalyst, the weight loss for Cu-Mn/TiO_2 and $Cu_1Mn_{0.5}Ti_{0.5}O_x$ became much less, which was 0.63 wt% and 0.39 wt% in step 2, and 1.31 wt% and 1.06 wt% in step 3, respectively. The results further demonstrated that less sulfate species was deposited on the surface of $Cu_1Mn_{0.5}Ti_{0.5}O_x$. The above results explains why $Cu_1Mn_{0.5}Ti_{0.5}O_x$ has better activity even in the presence of SO_2.

In order to explain the influence of SO_2, SO_2-TPD analyses were performed with $Cu_1Mn_{0.5}Ti_{0.5}O_x$, Cu-Mn/TiO_2, and Mn/TiO_2 after exposure to 5000 ppm SO_2 at 80 °C for 1 h, as shown in Fig. 10(c). For Mn/TiO_2, two SO_2 desorption peaks were observed at 292 and 542 °C. However, only one major SO_2 desorption peak appeared at 361 °C for $Cu_1Mn_{0.5}Ti_{0.5}O_x$ and 365 °C for Cu-Mn/TiO_2, which was due to the decomposition of sulfate species [62,63]. The SO_2-TPD peak of Mn/TiO_2 is much larger than that for $Cu_1Mn_{0.5}Ti_{0.5}O_x$, indicating $Cu_1Mn_{0.5}Ti_{0.5}O_x$ has excellent SO_2-resistant capacity. The deactivation of catalysts can be attributed to the sulfate species formation, which is consistent with the TGA analysis. In addition, the SO_2-desorption temperature of $Cu_1Mn_{0.5}Ti_{0.5}O_x$ is much lower than that of Mn/TiO_2, and this will be very beneficial for the catalyst regeneration process.

In addition, the $SO_2 + NH_3 + O_2$-TPD analyses of samples were used to clarify sulfate species. $Cu_1Mn_{0.5}Ti_{0.5}O_x$, Cu-Mn/TiO_2, and Mn/TiO_2 were exposed to 2500 ppm SO_2 and 2500 ppm NH_3 in the presence of 5% O_2 at 80 °C for 1 h, and all $SO_2 + NH_3 + O_2$-TPD results were shown in Fig. 10(d). For Mn/TiO_2, there are two desorption peaks at about 195 and 361 °C, which are attributed to the decomposition of $(NH_4)_2SO_4$/NH_4HSO_4 and sulfate species. For Cu-Mn/TiO_2 and $Cu_1Mn_{0.5}Ti_{0.5}O_x$, only one wide desorption peak (about 260 and 242 °C) attributable to $(NH_4)_2SO_4$/NH_4HSO_4 and sulfate species appeared, respectively. Obviously, it can be seen that the desorption peak of Mn/TiO_2 is much stronger than $Cu_1Mn_{0.5}Ti_{0.5}O_x$. Combining the in situ DRFT, SO_2-TPD, TGA, and $SO_2 + NH_3 + O_2$-TPD analyses, we can conclude that $Cu_1Mn_{0.5}Ti_{0.5}O_x$ has less $(NH_4)_2SO_4$/NH_4HSO_4 and sulfate species formation, indicating $Cu_1Mn_{0.5}Ti_{0.5}O_x$ has superior SO_2 resistance.

Fig. 11 shows the NO_x conversion of the deactivated catalysts after thermal regeneration. The NO_x conversion of fresh $Cu_1Mn_{0.5}Ti_{0.5}O_x$, Cu-Mn/TiO_2, and Mn/TiO_2 at 200 °C was 90%, 86.1%, and 80.7%, respectively. After 12 h of operation in the presence of 100 ppm SO_2, the NO_x conversions of $Cu_1Mn_{0.5}Ti_{0.5}O_x$, Cu-Mn/TiO_2, and Mn/TiO_2 catalysts decreased to 71.1%, 52.3%, and 41.5%, respectively. After thermal regeneration at 400 °C in air, the NO_x conversion of $Cu_1Mn_{0.5}Ti_{0.5}O_x$, Cu-Mn/TiO_2, and Mn/TiO_2 was recovered to 85.8%, 62.6%, and 51.8%, respectively. These results clearly indicated that $Cu_1Mn_{0.5}Ti_{0.5}O_x$ has much better regenerability and greater potential for practical applications than other catalysts.

3.2.3. Mechanism study

In all, the high activity of $CuMnTiO_x$ catalyst for NH_3-SCR at low-temperature could be attributed to high dispersion of manganese oxides and copper oxide with a high SSA, as well as the abundance of acid sites, etc. The NO oxidation reaction could be enhanced by the electron transferring, as shown in the following Eqs. (3)–(5) [64–67]. In addition, adding Cu can increase the amount of acid sites and enhance the SO_2 resistance of the Mn-based NH_3-SCR catalysts. Based the all the above results, a redox cycle for the NH_3-SCR reaction at low temperatures over this novel $CuMnTiO_x$ catalyst can be proposed, as described in Fig. 12. The NH_3-SCR reaction mechanism over $CuMnTiO_x$ could be explained by the E-R mechanism and L-H mechanism [68–70]. The coordinated NH_3 on the Lewis acid sites and the NH_4^+ on the Brønsted acid sites can react with gaseous NO (E-R mechanism) and the adsorbed

NO (L-H mechanism) over the $CuMnTiO_x$ catalyst. In E-R mechanism, the absorbed NH_3 species is converted to NH_2 species, and then reacts with gaseous NO to form highly active NH_4NO_2/NH_2NO intermediate. After that, NH_4NO_2/NH_2NO is unstable and decompose rapidly into N_2 and H_2O. While in the L-H mechanism, the NH_3-SCR reaction occurs between adsorbed NH_3 species and adsorbed NO species.

$$Mn^{4+} + NO \rightarrow Mn^{3+} + NO_{ads}{}^{+} \quad (3)$$

$$Cu^{+} + 0.5O_2 \rightarrow Cu^{2+} + O_{ads}{}^{-} \quad (4)$$

$$NO_{ads}{}^{+} + O_{ads}{}^{-} \rightarrow NO_2 \quad (5)$$

4. Conclusions

We designed a series of novel low-temperature NH_3-SCR catalysts $Cu_wMn_yTi_{1-y}O_x$ containing CuO and MnO_x as active components and TiO_2 as support from $Cu_wMn_yTi_{1-y}$-CO_3 LDHs precursors. The optimal sample $Cu_1Mn_{0.5}Ti_{0.5}O_x$ displayed a high De-NO_x efficiency of 90% at 200 °C, higher than that for 20 wt% Mn/TiO_2 (80.7%), 10 wt% Cu-10 wt% Mn/TiO_2 (86.1%), 20 wt% Cu-20 wt% Mn/TiO_2 (80.2%), and 40 wt% Cu-20 wt% Mn/TiO_2 (60.3%). XRD, HR-TEM, and XPS analyses showed that the $Cu_1Mn_{0.5}Ti_{0.5}O_x$ sample contains highly dispersed MnO_2 and CuO phases, which may be partly responsible for its good performance. NH_3-TPD, Py-FTIR, in situ DRIFT, and H_2-TPR results suggested that $Cu_1Mn_{0.5}Ti_{0.5}O_x$ possesses more acid sites and surface active species than other samples studied in this work. In addition, $Cu_1Mn_{0.5}Ti_{0.5}O_x$ has excellent resistance to SO_2 and H_2O, and its aged sample has better regenerability, suggesting a greater potential for practical applications.

Acknowledgements

This work was supported by the National Natural Science Foundation of China (51622801, 51572029), and the Beijing Excellent Young Scholar (2015000026833ZK11).

Appendix A. Supplementary data

Supplementary material related to this article can be found, in the online version, at doi:https://doi.org/10.1016/j.apcatb.2018.07.035.

References

[1] I. Nova, C. Ciardelli, E. Tronconi, D. Chatterjee, B. Bandl-Konrad, NH_3-NO/NO_2 chemistry over V-based catalysts and its role in the mechanism of the fast SCR reaction, Catal. Today 114 (2006) 3–12.
[2] W.S. Kijlstra, D.S. Brands, E.K. Poels, A. Bliek, Mechanism of the selective catalytic reduction of NO by NH_3 over MnO_x/Al_2O_3, J. Catal. 171 (1997) 208–218.
[3] X. Tang, J. Hao, H. Yi, J. Li, Low-temperature SCR of NO with NH_3 over AC/C supported manganese-based monolithic catalysts, Catal. Today 126 (2007) 406–411.
[4] Y.J. Kim, H.J. Kwon, I.S. Nam, J.W. Choung, J.K. Kil, H.J. Kim, M. Cha, G.K. Yeo, High deNO_x performance of Mn/TiO_2 catalyst by NH_3, Catal. Today 151 (2010) 244–250.
[5] R.Q. Long, R.T. Yang, R. Chang, Low temperature selective catalytic reduction (SCR) of NO with NH_3 over Fe-Mn based catalysts, Chem. Commun. 5 (2002) 452–453.
[6] A. Sultana, M. Sasaki, H. Hamada, Influence of support on the activity of Mn supported catalysts for SCR of NO with ammonia, Catal. Today 185 (2012) 284–289.
[7] S. Roy, M.S. Hegde, G. Madras, Catalysis for NO_x abatement, Appl. Energy 86 (2009) 2283–2297.
[8] P.G. Smirniotis, D.A. Pena, B.S. Uphade, Low-temperature selective catalytic reduction (SCR) of NO with NH_3 by using Mn, Cr, and Cu oxides supported on hombikat TiO_2, Angew. Chem. Int. Ed. 40 (2001) 2479–2482.
[9] K. Shen, Y. Zhang, X. Wang, H. Xu, K. Sun, C. Zhou, Influence of chromium modification on the properties of MnO_x-FeO_x catalysts for the low-temperature selective catalytic reduction of NO by NH_3, J. Energy Chem. 22 (2013) 617–623.
[10] Z. Wu, B. Jiang, Y. Liu, Effect of transition metals addition on the catalyst of manganese/titania for low-temperature selective catalytic reduction of nitric oxide with ammonia, Appl. Catal. B: Environ. 79 (2008) 347–355.
[11] J. Li, H. Chang, L. Ma, J. Hao, R.T. Yang, Low-temperature selective catalytic reduction of NO_x with NH_3 over metal oxide and zeolite catalysts-a review, Catal. Today 175 (2011) 147–156.
[12] S. Roy, B. Viswanath, M.S. Hegde, G. Madras, Low-temperature selective catalytic reduction of NO with NH_3 over Ti0. $9M_{0.\ 1}O_{2-\delta}$ (M = Cr, Mn, Fe, Co, Cu), J. Phys. Chem. C 112 (2008) 6002–6012.
[13] R. Zhang, X. Wang, S. Yu, T. Wen, X. Zhu, F. Yang, X. Sun, X. Wang, W. Hu, Ternary $NiCo_2P_x$ nanowires as pH-universal electrocatalysts for highly efficient hydrogen evolution reaction, Adv. Mater. 29 (2017) 1605502.
[14] G. Zhao, X. Huang, X. Wang, X. Wang, Progress in catalyst exploration for heterogeneous CO_2 reduction and utilization: a critical review, J. Mater. Chem. A 5 (2017) 21625–21649.
[15] B. Bridier, N. López, J. Pérez-Ramírez, Partial hydrogenation of propyne over copper-based catalysts and comparison with nickel-based analogues, J. Catal. 269 (2010) 80–92.
[16] J.H. Kwak, D. Tran, S.D. Burton, J. Szanyi, J.H. Lee, C.H. Peden, Effects of hydrothermal aging on NH_3-SCR reaction over Cu/zeolites, J. Catal. 287 (2012) 203–209.
[17] J. Xue, X. Wang, G. Qi, J. Wang, M. Shen, W. Li, Characterization of copper species over Cu/SAPO-34 in selective catalytic reduction of NO_x with ammonia: relationships between active Cu sites and de-NO_x performance at low temperature, J. Catal. 297 (2013) 56–64.
[18] P.A. Kumar, M.P. Reddy, L.K. Ju, B. Hyun-Sook, H.H. Phil, Low temperature propylene SCR of NO by copper alumina catalyst, J. Mol. Catal. A Chem. 291 (2008) 66–74.
[19] V. Houel, D. James, P. Millington, S. Pollington, S. Poulston, R. Rajaram, R. Torbati, A comparison of the activity and deactivation of Ag/Al_2O_3 and Cu/ZSM-5 for HC-SCR under simulated diesel exhaust emission conditions, J. Catal. 230 (2005) 150–157.
[20] B. Liu, Y. Liu, C. Li, W. Hu, P. Jing, Q. Wang, J. Zhang, Three-dimensionally ordered macroporous Au/CeO_2-Co_3O_4 catalysts with nanoporous walls for enhanced catalytic oxidation of formaldehyde, Appl. Catal. B: Environ. 127 (2012) 47–58.
[21] Q. Wang, S.V.Y. Tang, E. Lester, D. O'Hare, Synthesis of ultrafine layered double hydroxide (LDHs) nanoplates using a continuous-flow hydrothermal reactor, Nanoscale 5 (2013) 114–117.
[22] J. Wang, X. Mei, L. Huang, Q. Zheng, Y. Qiao, K. Zang, S. Mao, R. Yang, Z. Zhang, Y. Gao, Z. Guo, Z. Huang, Q. Wang, Synthesis of layered double hydroxides/graphene oxide nanocomposite as novel high-temperature CO_2 adsorbent, J. Energy Chem. 24 (2015) 127–137.
[23] Q. Qin, J. Wang, T. Zhou, Q. Zheng, L. Huang, Y. Zhang, P. Lu, A. Umar, B. Louis, Q. Wang, Impact of organic interlayer anions on the CO_2 adsorption performance of Mg-Al layered double hydroxides derived mixed oxides, J. Energy Chem. 26 (2017) 346–353.
[24] J. Wang, Y. Yang, L. Jia, N. Yang, Q. Guan, L. Huang, A. Umar, Q. Wang, P. Ning, The influence of the charge compensating anions of layered double hydroxides (LDHs) in LDH-NS/Graphene oxide nanohybrid for CO_2 capture, J. Nanosci. Nanotechnol. 18 (2018) 2956–2964.
[25] Q. Yan, S. Chen, C. Zhang, D. O'Hare, Q. Wang, Synthesis of $Cu_{0.5}Mg_{1.5}Mn_{0.5}Al_{0.5}O_x$ mixed oxide from layered double hydroxide precursor as highly efficient catalyst for low-temperature selective catalytic reduction of NO_x with NH_3, J. Colloid Interface Sci. 526 (2018) 63–74.
[26] Y. Nie, Q. Yan, S. Chen, D. O'Hare, Q. Wang, CuTi LDH derived NH_3-SCR catalysts with highly dispersed CuO active phase and improved SO_2 resistance, Catal. Commun. 97 (2017) 47–50.
[27] R. Yang, Y. Cui, Q. Yan, C. Zhang, L. Qiu, D. O'Hare, Q. Wang, Design of highly efficient NO_x storage-reduction catalysts from layered double hydroxides for NO_x emission control from naphtha cracker flue gases, Chem. Eng. J. 326 (2017) 656–666.
[28] M.H. Yao, R.J. Baird, F.W. Kunz, T.E. Hoost, An XRD and TEM investigation of the structure of alumina-supported Ceria-Zirconia, J. Catal. 166 (1997) 67–74.
[29] Q. Wang, H.H. Tay, D.J.W. Ng, L. Chen, Y. Liu, J. Chang, Z. Zhong, J. Luo, A. Borgna, The effect of trivalent cations on the performance of Mg-M-CO_3 layered double hydroxides for high-temperature CO_2 capture, ChemSusChem 3 (2010) 965–973.
[30] C.J. Wang, D. O'Hare, Topotactic synthesis of layered double hydroxide nanorods, J. Mater. Chem. 22 (2012) 23064–23070.
[31] P. Zhang, G. Qian, Z.P. Xu, H. Shi, X. Ruan, J. Yang, R.L. Frost, Effective adsorption of sodium dodecylsulfate (SDS) by hydrocalumite (CaAl-LDH-Cl) induced by self-dissolution and re-precipitation mechanism, J. Colloid Interface Sci. 367 (2012) 264–271.
[32] Y. Gao, Z. Zhang, J. Wu, X. Yi, A. Zheng, A. Umar, D. O'Hare, Q. Wang, Comprehensive investigation of CO_2 adsorption on Mg-Al-CO_3 LDH-derived mixed metal oxides, J. Mater. Chem. A 1 (2013) 12782–12790.
[33] X. Tang, J. Li, L. Sun, J. Hao, Origination of N_2O from NO reduction by NH_3 over β-MnO_2 and α-Mn_2O_3, Appl. Catal. B: Environ. 99 (2010) 156–162.
[34] Y. Wu, Y. Lu, C. Song, Z. Ma, S. Xing, Y. Gao, A novel redox-precipitation method for the preparation of α-MnO_2 with a high surface Mn^{4+} concentration and its activity toward complete catalytic oxidation of o-xylene, Catal. Today 201 (2013) 32–39.
[35] S.S.R. Putluru, L. Schill, A.D. Jensen, B. Siret, F. Tabaries, R. Fehrmann, Mn/TiO_2 and Mn-Fe/TiO_2 catalysts synthesized by deposition precipitation-promising for selective catalytic reduction of NO with NH_3 at low temperatures, Appl. Catal. B: Environ. 165 (2015) 628–635.
[36] Y. Wang, B. Li, C. Zhang, L. Cui, S. Kang, X. Li, L. Zhou, Ordered mesoporous CeO_2-TiO_2 composites: highly efficient photocatalysts for the reduction of CO_2 with H_2O under simulated solar irradiation, Appl. Catal. B: Environ. 130–131 (2013) 277–284.
[37] X. Gao, Y. Jiang, Y. Zhong, Z. Luo, K. Cen, The activity and characterization of CeO_2-TiO_2 catalysts prepared by the sol-gel method for selective catalytic reduction

of NO with NH_3, J. Hazard. Mater. 174 (2010) 734–739.
[38] C. Fang, D. Zhang, S. Cai, L. Zhang, L. Huang, H. Li, P. Maitarad, L. Shi, R. Gao, J. Zhang, Low-temperature selective catalytic reduction of NO with NH_3 over nanoflaky MnO_x on carbon nanotubes in situ prepared via a chemical bath deposition route, Nanoscale 5 (2013) 9199–9207.
[39] L. Chen, J. Li, M. Ge, The poisoning effect of alkali metals doping over nano V_2O_5-WO_3/TiO_2 catalysts on selective catalytic reduction of NO_x by NH_3, Chem. Eng. J. 170 (2011) 531–537.
[40] Q. Li, H. Yang, F. Qiu, X. Zhang, Promotional effects of carbon nanotubes on V_2O_5/TiO_2 for NO_x removal, J. Hazard. Mater. 192 (2011) 915–921.
[41] F. Liu, H. He, C. Zhang, Z. Feng, L. Zheng, Y. Xie, T. Hu, Selective catalytic reduction of NO with NH_3 over iron titanate catalyst: catalytic performance and characterization, Appl. Catal. B: Environ. 96 (2010) 408–420.
[42] M.I. Zaki, M.A. Hasan, F.A. Al-Sagheer, L. Pasupulety, In situ FTIR spectra of pyridine adsorbed on SiO_2-Al_2O_3, TiO_2, ZrO_2 and CeO_2: general considerations for the identification of acid sites on surfaces of finely divided metal oxides, Colloid. Surf. A 190 (2001) 261–274.
[43] N. Li, A. Wang, M. Zheng, X. Wang, R. Cheng, T. Zhang, Probing into the catalytic nature of Co/sulfated zirconia for selective reduction of NO with methane, J. Catal. 225 (2004) 307–315.
[44] P. Kalita, N.M. Gupta, R. Kumar, Synergistic role of acid sites in the Ce-enhanced activity of mesoporous Ce-Al-MCM-41 catalysts in alkylation reactions: FTIR and TPD-ammonia studies, J. Catal. 245 (2007) 338–347.
[45] J. Zhu, F. Gao, L. Dong, W. Yu, L. Qi, Z. Wang, L. Dong, Y. Chen, Studies on surface structure of $M_xO_y/MoO_3/CeO_2$ system (M= Ni, Cu, Fe) and its influence on SCR of NO by NH_3, Appl. Catal. B: Environ. 95 (2010) 144–152.
[46] B. Jiang, B. Deng, Z. Zhang, Z. Wu, X. Tang, S. Yao, H. Lu, Effect of Zr addition on the low-temperature SCR activity and SO_2 tolerance of Fe-Mn/Ti catalysts, J. Phys. Chem. C 118 (2014) 14866–14875.
[47] C. Sun, J. Zhu, Y. Lv, Dispersion, reduction and catalytic performance of CuO supported on ZrO_2-doped TiO_2 for NO removal by CO, Appl. Catal. B: Environ. 103 (2011) 206–220.
[48] S. Guerrero, I. Guzmán, G. Aguila, Sodium-promoted NO adsorption under lean conditions over Cu/TiO_2 catalysts, Catal. Commun. 11 (2009) 38–42.
[49] Y. Xiong, C. Tang, X. Yao, L. Zhang, L. Li, X. Wang, Y. Deng, F. Gao, L. Dong, Effect of metal ions doping (M = Ti^{4+}, Sn^{4+}) on the catalytic performance of MnO_x/CeO_2 catalyst for low temperature selective catalytic reduction of NO with NH_3, Appl. Catal. A: Gen. 495 (2015) 206–216.
[50] Z. Huang, Z. Zhu, Z. Liu, Combined effect of H_2O and SO_2 on V_2O_5/AC catalysts for NO reduction with ammonia at lower temperatures, Appl. Catal. B Environ. 39 (2002) 361–368.
[51] X. Lu, C. Song, S. Jia, Z. Tong, X. Tang, Y. Teng, Low-temperature selective catalytic reduction of NO_x with NH_3 over cerium and manganese oxides supported on TiO_2-graphene, Chem. Eng. J. 260 (2015) 776–784.
[52] T. Yamaguchi, T. Jin, K. Tanabe, Structure of acid sites on sulfur-promoted iron oxide, J. Phys. Chem. C 90 (1986) 3148–4152.
[53] M. Waqif, P. Bazin, O. Saur, J.C. Lavalley, G. Blanchard, O. Touret, Study of ceria sulfation, Appl. Catal. B: Environ. 11 (1997) 193–205.
[54] L. Zhang, J. Pierce, V.L. Leung, D. Wang, W.S. Epling, Characterization of Ceria's interaction with NO_x and NH_3, J. Phys. Chem. C 117 (2013) 8282–8289.
[55] S.D. Lin, A.C. Gluhoi, B.E. Nieuwenhuys, Ammonia oxidation over $Au/MO_x/\gamma$-Al_2O_3-activity, selectivity and FTIR measurements, Catal. Today 90 (2004) 3–14.
[56] G. Qi, R.T. Yang, R. Chang, MnO_x-CeO_2 mixed oxides prepared by co-precipitation for selective catalytic reduction of NO with NH_3 at low temperatures, Appl. Catal. B: Environ. 51 (2004) 93–106.
[57] L. Zhang, D. Wang, Y. Liu, K. Kamasamudram, J. Li, W.S. Epling, SO_2 poisoning impact on the NH_3-SCR reaction over a commercial Cu-SAPO-34 SCR catalyst, Appl. Catal. B Environ. 156–157 (2014) 371–377.
[58] R. Jin, Y. Liu, Z. Wu, H. Wang, T. Gu, Relationship between SO_2 poisoning effects and reaction temperature for selective catalytic reduction of NO over Mn-Ce/TiO_2 catalyst, Catal. Today 153 (2010) 84–89.
[59] J. Eng, C.H. Bartholomew, Kinetic and mechanistic study of NO_x reduction by NH_3 over H-form zeolites, J. Catal. 171 (1997) 27–44.
[60] K. Wijayanti, S. Andonova, A. Kumar, J. Li, K. Kamasamudram, N.W. Currier, A. Yezerets, L. Olsson, Impact of sulfur oxide on NH_3-SCR over Cu-SAPO-34, Appl. Catal. B Environ. 166–167 (2015) 568–579.
[61] D.W. Kwon, K.B. Nam, S.C. Hong, The role of ceria on the activity and SO_2 resistance of catalysts for the selective catalytic reduction of NO_x by NH_3, Appl. Catal. B: Environ. 166–167 (2015) 37–44.
[62] M. Waqif, O. Saur, J.C. Lavalley, S. Perathoner, G. Centi, Nature and mechanism of formation of sulfate specles on copper/alumlna sorbent-catalysts for SO_2 removal, J. Phys. Chem. 95 (1991) 4051–4058.
[63] K.S. Yoo, S.D. Kim, S.B. Park, Sulfation of Al_2O_3 in flue gas desulfurization by CuO/y-Al_2O_3 sorbent, Ind. Eng. Chem. Res. 33 (1994) 1786–1791.
[64] M. Kang, E.D. Park, J.M. Kim, J.E. Yie, Cu-Mn mixed oxides for low temperature NO reduction with NH_3, Catal. Today 111 (2006) 236–241.
[65] S. Vepřek, D.L. Cocke, S. Kehl, H.R. Oswald, Mechanism of the deactivation of hopcalite catalysts studied by XPS, ISS, and other techniques, J. Catal. 100 (1986) 250–263.
[66] Z. Chen, Q. Yang, H. Li, X. Li, L. Wang, S.C. Tsang, Cr-MnO_x mixed-oxide catalysts for selective catalytic reduction of NO_x with NH_3 at low temperature, J. Catal. 276 (2010) 56–65.
[67] F.C. Buciuman, F. Patcas, T. Hahn, A spillover approach to oxidation catalysis over copper and manganese mixed oxides, Chem. Eng. Process. 38 (1999) 563–569.
[68] Y. Chen, J. Wang, Z. Yan, L. Liu, Z. Zhang, X. Wang, Promoting effect of Nd on the reduction of NO with NH_3 over CeO_2 supported by activated semi-coke: an in situ DRIFTS study, Catal. Sci. Technol. 5 (2015) 2251–2259.
[69] L. Chen, J. Li, M. Ge, DRIFT study on cerium-tungsten/titiania catalyst for selective catalytic reduction of NO_x with NH_3, Environ. Sci. Technol. 44 (2010) 9590–9596.
[70] N. Yang, R. Guo, W. Pan, Q. Chen, Q. Wang, C. Lu, S. Wang, The deactivation mechanism of Cl on Ce/TiO_2 catalyst for selectivecatalytic reduction of NO with NH_3, Appl. Surf. Sci. 378 (2016) 513–518.